High-Resolution Probe of Coherence in Low-Energy Charge Exchange Collisions with Oriented Targets

A. Leredde,[1] X. Fléchard,[1] A. Cassimi,[2] D. Hennecart,[2] and B. Pons[3]
[1]LPC Caen, ENSICAEN, Université de Caen, CNRS/IN2P3, F-14070 Caen, France
[2]CIMAP, CEA—CNRS—ENSICAEN, BP 5133, F-14070 Caen cedex 5, France
[3]CELIA, Université Bordeaux—CNRS—CEA, F-33405 Talence, France
(Received 16 May 2013; revised manuscript received 9 August 2013; published 26 September 2013)

The trapping lasers of a magneto-optical trap have been used to bring Rb atoms into well defined oriented states. Coupled to recoil-ion-momentum spectroscopy, this provided a unique MOTRIMS setup which was able to probe scattering dynamics, including the coherence features, with unprecedented resolution. The technique was applied to the low-energy charge exchange reactions $Na^+ + Rb(5p_{\pm 1}) \rightarrow Na(3p, 4s) + Rb^+$. The measurements revealed detailed features of the collisional interaction which were employed to improve the theoretical description. As such, it was possible to ascertain the validity of the intuitive models used to predict the most likely capture transitions.

DOI: 10.1103/PhysRevLett.111.133201 PACS numbers: 34.70.+e, 34.10.+x, 37.10.Gh

Understanding the dynamics underlying nonadiabatic processes in atomic and molecular physics becomes particularly difficult as soon as multiple pathways link the same initial and final states. Beyond the identification of the various reaction routes, their relative coherence must be considered explicitly as it controls the occurrence of interferences and therefore determines the final outcome of the reaction. Coherence parameters have been obtained from "quantum mechanically complete" experiments [1] for low-energy ion-atom collisions [2–9], electron impact excitation of helium [10,11], and strong-field ionization of krypton atoms [12]. Nevertheless, in most of the cases involving heavy particles, the experimental resolution did not permit the details of the scattering patterns predicted theoretically to be explored.

Here, we demonstrate that scattering dynamics, including their coherence and interferential features, can be probed with unprecedented resolution by coupling recoil-ion-momentum spectroscopy (RIMS [13]) to laser-cooled targets trapped in a magneto-optical trap (MOT) [14–20]. Moreover, we have designed a novel MOT setup in which the trapping laser pulses are employed to selectively orient the target states. This enables the observation of coherent dynamics from a single excited state.

Magneto-optical trap recoil-ion-momentum spectroscopy (MOTRIMS) can in principle be employed, as in conventional RIMS, to probe a multitude of scattering dynamics [13]. We focus herein on the case of charge exchange scattering between Na^+ ions and excited $Rb(5p_{\pm 1})$ targets in the keV energy range. It is known from previous studies on similar systems [2–9,21–23] that the differential cross sections (DCS) for charge exchange exhibit pronounced asymmetries related to the coherence of the capture process (Fig. 1). However, most of these previous studies called for more precise measurements in order to reveal the exact angular dependance of the DCS and associated coherence parameters. In this respect, $Na^+ + Rb$ collisions are particularly challenging since the projectiles are scattered in very forward directions [18]. We prove that the MOTRIMS technique achieves the required resolution and therefore provides, concurrently with calculations, a detailed picture of the underlying dynamics, beyond our basically classical intuition.

Our MOTRIMS setup has been described in detail elsewhere [17,18]. We therefore focus here on the modifications we made to combine efficient orientation and RIMS techniques within a MOT.

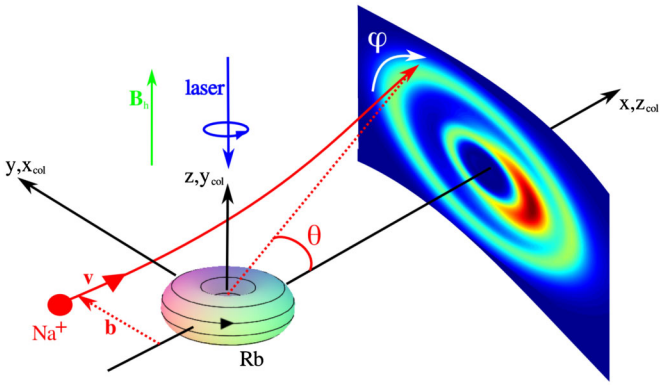

FIG. 1 (color online). Schematic representation of the experiment. A homogeneous magnetic field B_h defines the quantization direction (z axis), and optical pumping leads to magnetic sublevels of the target state with well defined hyperfine quantum numbers m_F, depending on the handedness of the laser pulse. The initial and final states are therefore quantized in the (x, y, z) reference frame. The Na^+ ions impinge on the oriented target with velocity $\mathbf{v}$ and impact parameter $\mathbf{b}$, and the scattered projectile distribution is characterized by the spherical angles (θ, φ) in the (x_{col}, y_{col}, z_{col}) scattering frame.

The high-resolution performance of our MOTRIMS setup relies on the transverse extraction of the recoil ions coupled to a fast switch-off of the trapping magnetic field just prior to the data taking [18]. The field-free requirement is important, as any weak parasitic magnetic fields, including Earth's, can affect the alignment, which has to be fixed. The total angular momentum of the target was thus unambiguously aligned, for both the ground $\mathrm{Rb}(5^2S_{1/2}, F = 2)$ and excited $\mathrm{Rb}(5^2P_{3/2}, F' = 3)$ states, by using a homogeneous magnetic field B_h along the z axis which is taken as the quantization direction (Fig. 1). The field B_h is provided by Helmotz coils, and its magnitude is 2 G, which is large enough to negate any perturbing magnetic field. To compensate for the effects of B_h during the trapping period, the position of one of the MOT anti-Helmotz coils was raised by 4 mm.

To bring the $\mathrm{Rb}(5^2S_{1/2}, F = 2)$ and $\mathrm{Rb}(5^2P_{3/2}, F' = 3)$ atoms into oriented $m_F = +2$ and $m'_F = +3$ magnetic substates, respectively, we optically pumped them using a left-handed circularly polarized laser beam, along the $-z$ direction, that induced σ^+ transitions. The opposite orientation was obtained using a right-handed laser beam. The polarizing laser beam (PLB), coming from one of the trapping lasers, is diffracted by an acousto-optic modulator and tuned slightly to the red side of the $(5^2S_{1/2}, F = 2) \rightarrow (5^2P_{3/2}, F' = 3)$ transition. This acousto-optic modulator can be switched *on* and *off* to control the status of the PLB. A half-wave plate coupled to a polarizing beam splitting cube provided a linearly polarized beam with tunable intensity. The beam was circularly polarized using a quarter-wave plate and directed towards the target. A counterpropagating laser beam, obtained by retroreflection at the exit side of the collision chamber, reduced the net momentum transfer from the PLB to the target atoms. In spite of this retroreflected beam, the cold cloud was still warmed up and lost after a few ms with a time constant depending on the intensities and alignment of the laser beams. An incoming laser beam with a power of 1 $\mathrm{mW/cm^2}$ was thus used to prepare a target with a large fraction of excited atoms without pushing the cloud outside of the collision region.

The polarization speed and orientation yield were characterized by means of absorption and fluorescence techniques, respectively. We found that more than 95% of the atoms were oriented within a time interval shorter than 5 μs. Experiments were performed with oriented $\mathrm{Rb}(5^2P_{3/2}, F = 3, m_F = \pm 3) \equiv \mathrm{Rb}(5p_{\pm 1})$ targets at $E = 5$, 2, and 1 keV. The capture channels of interest $\mathrm{Na}^+ + \mathrm{Rb}(5p_{\pm 1}) \rightarrow \mathrm{Na}(nl) + \mathrm{Rb}^+$ were easily identified and selected using the recoil-ion-momentum component parallel to the projectile beam axis. Precise DCS in projectile scattering angles θ and φ (Fig. 1) were then derived from the transverse momentum components [17,18].

We present in Figs. 2(a)–2(f) the weighted DCS $\sin(\theta)\sigma_{p_{+1}\rightarrow 3p}(\theta, \varphi)$ associated with the principal

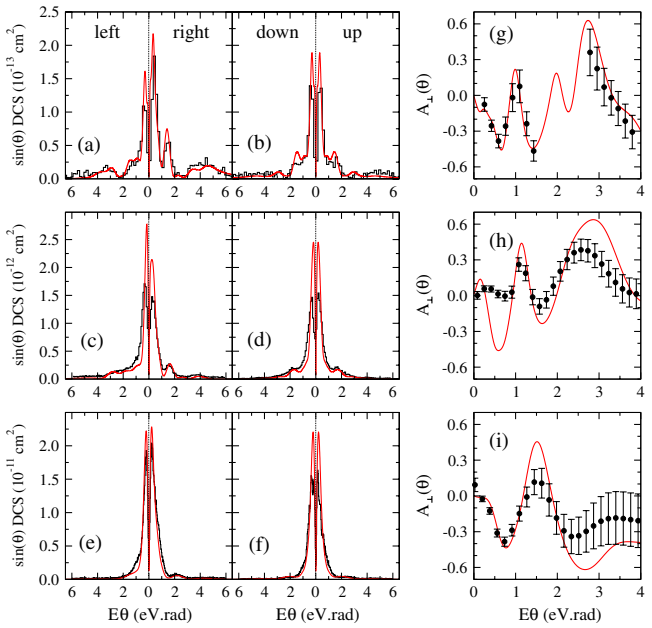

FIG. 2 (color online). Weighted DCSs for the charge exchange reaction $\mathrm{Na}^+ + \mathrm{Rb}(5p_{+1}) \rightarrow \mathrm{Na}(3p) + \mathrm{Rb}^+$ at $E = 1$ [(a),(b)], 2 [(c),(d)], and 5 [(e),(f)] keV, as functions of $E\theta$. The histograms are the measurements, while the continuous (red) lines correspond to MOCC calculations. In (g), (h), and (i), the left-right coherence parameters $A_\perp(\theta)$, as defined in Eq. (2), are displayed for $E = 1$, 2, and 5 keV.

$\mathrm{Na}^+ + \mathrm{Rb}(5p_{+1}) \rightarrow \mathrm{Na}(3p) + \mathrm{Rb}^+$ charge exchange reaction, in terms of its four main contributions to which we refer to as left ($\varphi = 0$), up ($\varphi = \pi/2$), right ($\varphi = \pi$), and down ($\varphi = 3\pi/2$) (Fig. 1 and Ref. [24]). These contributions are displayed as functions as $E\theta$, which is related to the impact parameter b characterizing the incoming projectile trajectories through the classical relationship $b \propto 1/E\theta$ [25]. The main peaks of the $\mathrm{Rb}(5p_{+1}) \rightarrow \mathrm{Na}(3p)$ DCS are roughly located at the same $E\theta$ values, regardless of E between 1 and 5 keV; this indicates that the main capture transitions occur at the same impact parameter in the (restricted) energy range considered.

We observe in Fig. 2 that the up and down contributions to the DCS are symmetric, whereas the left and right ones exhibit strong asymmetry. As may be seen from Fig. 1, the rotation of the electron flow inherent to the initial oriented state breaks the symmetry of left ($y > 0$) and right ($y < 0$) scatterings while it preserves the up-down symmetry because of reflection symmetry with respect to the (x, y) plane. To proceed more quantitatively, the quantum-mechanical origin of the asymmetry must be considered.

As shown schematically in Fig. 1, the initial and final atomic states are indeed quantized in the laboratory-fixed reference frame (x, y, z) related to the geometrical configuration of the orientation setup. However, as soon as the Na^+ beam impinges on Rb, the two-center Na-Rb scattering is naturally described in the (x_{col}, y_{col}, z_{col}) collisional

frame in which the scattering states exhibit cylindrical symmetry with respect to the direction of the incoming beam. Therefore, multiple collisional pathways are generally involved in a single charge exchange transition, as the initial and final oriented states, which do not present the appropriate collisional symmetry, are linear combinations of scattering states defined in the ($x_{\rm col}$, $y_{\rm col}$, $z_{\rm col}$) frame. These pathways may interfere, depending on their relative coherence, and yield strongly asymmetric DCS for the scattered projectiles.

In this work, our measurements are compared to the molecular orbital close-coupling (MOCC) calculations detailed in Ref. [18]. Briefly MOCC is a semiclassical approach which combines a classical description of nuclear motion and a quantum-mechanical description of electron transitions. We employ the single-active-electron (Ref. [25]) approximation where only nonadiabatic transitions involving the Rb valence electron are considered and both the Rb^+ target and Na^+ projectile atomic cores are assumed to remain frozen throughout the collision. The description of the Na^+-Rb^+ core-core interaction is first restricted to its Coulombic repulsive part $1/R(t)$, where $R(t)$ is the time-dependent internuclear distance, as usual in treatments of collisions with a dressed target and projectile (see, for example, Refs. [21,22]). MOCC employs the real orbitals $\{p_x, p_y, p_z\}$ in the ($x_{\rm col}$, $y_{\rm col}$, $z_{\rm col}$) frame and gives the scattering amplitudes $T_{p_{x,y,z}\to p_{x,y,z}}(\theta)$ in the collisional (v, b) plane. The $\mathrm{Rb}(5p_{+1}) \to \mathrm{Na}(3p)$ DCS is then expressed as

$$\begin{aligned}\sigma_{p_{+1}\to 3p}(\theta,\varphi) = (1/2)\{&|T_{p_z\to p_z}|^2 + |T_{p_z\to p_x}|^2 \\ &+ \cos^2(\varphi)(|T_{p_x\to p_x}|^2 + |T_{p_x\to p_z}|^2) \\ &+ \sin^2(\varphi)|T_{p_y\to p_y}|^2\} \\ &+ \cos(\varphi)\,\mathrm{Im}(T_{p_z\to p_z}T^*_{p_x\to p_z} - T_{p_x\to p_x}T^*_{p_z\to p_x}).\end{aligned} \tag{1}$$

One can distinguish in Eq. (1) the incoherent part of the $5p_{+1} \to 3p$ process, in terms of noninteracting collisional pathways grouped in the brackets, from the interferential contribution involving products of different T amplitudes.

The agreement between the experimental and computed DCS displayed in Figs. 2(a)–2(f) is very satisfactory. The positions of the theoretical DCS peaks coincide with those obtained experimentally, which confirms that MOCC reliably describes the transition dynamics. However, the MOCC peaks are somewhat higher in amplitude and narrower than the measurements. These slight discrepancies arise as the calculations have been convoluted with an angular resolution $\Delta\theta$ which does not account for the experimental polarization procedure [26]. The left/(right + left) total ratios $R = \int \sin(\theta)\sigma_{p_{+1}\to 3p}(\theta, 0)d\theta \,/ \int \sin(\theta)[\sigma_{p_{+1}\to 3p}(\theta, 0) + \sigma_{p_{+1}\to 3p}(\theta, \pi)]d\theta$ derived from the measurements and MOCC calculations are, however, in striking agreement. For instance, $R^{\rm MOTRIMS} = 37.7\%$ and $R^{\rm MOCC} = 37.5\%$ at $E = 1$ keV. Furthermore, and importantly, the exceptional angular resolution provided by the setup (varying from 70 μrad at 1 keV to 28 μrad at 5 keV) enabled the oscillatory patterns of the DCS and associated (θ-dependent) left-right asymmetry to be resolved. This would have been clearly impossible with conventional setups where angular resolution is rather $\Delta\theta \sim 1$ mrad. By analogy with the contrast of interference fringes, which is employed in Young's slit experiments to determine the coherence of light waves passing through slits, we define the θ-dependent left-right asymmetry parameter $A_\perp(\theta) = [\sigma_{p_{+1}\to 3p}(\theta,0) - \sigma_{p_{+1}\to 3p}(\theta,\pi)]/[\sigma_{p_{+1}\to 3p}(\theta,0) + \sigma_{p_{+1}\to 3p}(\theta,\pi)]$. $A_\perp$ gives direct access to the degree of coherence of the $\mathrm{Rb}(5p_{+1}) \to \mathrm{Na}(3p)$ charge exchange mechanism. In particular, it measures the importance of interference effects between "radial" ($p_z \to p_z$, $p_x \to p_x$) and "rotational" ($p_z \to p_x$, $p_x \to p_z$) collisional transition pathways, since one obtains from Eq. (1)

$$A_\perp(\theta) = \frac{2\,\mathrm{Im}(T_{p_z\to p_z}T^*_{p_x\to p_z} - T_{p_x\to p_x}T^*_{p_z\to p_x})}{|T_{p_z\to p_z}|^2 + |T_{p_x\to p_x}|^2 + |T_{p_z\to p_x}|^2 + |T_{p_x\to p_z}|^2}. \tag{2}$$

$A_\perp(\theta)$ is presented in Figs. 2(g)–2(i) for $E = 1$, 2, and 5 keV. The overall agreement of the measured and predicted coherence pictures is satisfactory [27]. $|A_\perp|$ rapidly varies as a function of θ and it reaches values as high as 0.5. As E decreases, the interference pattern presents more structures within a fixed $E\theta$ range. This behavior stems from the fact that the phases of the scattering amplitudes are inversely proportional to the impact velocity v [18], which enhances the number of constructive and destructive occurrences in the T products of Eq. (2) as E decreases.

Our setup has allowed us to reliably extract from the raw data the signal associated with the secondary capture channel $\mathrm{Na}^+ + \mathrm{Rb}(5p_{+1}) \to \mathrm{Na}(4s) + \mathrm{Rb}^+$ at $E = 1$ keV. To our knowledge, no previous measurements were able to explore secondary transfer dynamics at the coherence level. The DCS and corresponding $A_\perp(\theta)$ are presented in Fig. 3. A double-ring structure is observed in the DCS which arises from $5p \to 4s$ transitions occurring at rather small internuclear distances $R < 12$ a.u. However, while the measurements yield a maximum outer ring for $\varphi = 0$, $\pi/2$, and $3\pi/2$, the MOCC calculations predict the opposite. This means that the model underestimates the $4s$ capture transitions at small b. We demonstrate in Fig. 3 that this is due to the inadequate representation of the core-core interaction in terms of purely Coulombic repulsion $1/R$. We have implemented improved MOCC calculations in which the mutual polarization of the Na^+ and Rb^+ cores is accounted by attractive ion-dipole $-(\alpha_d^{\mathrm{Rb}^+} + \alpha_d^{\mathrm{Na}^+})/2R^4$ and dipole-dipole $-(\alpha_q^{\mathrm{Rb}^+} + \alpha_q^{\mathrm{Na}^+})/2R^6$ potentials, where α_d and α_q are the dipole and quadrupole polarizabilities of

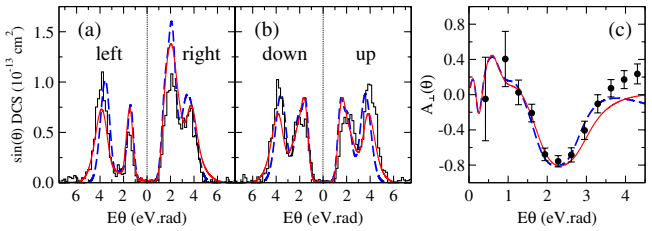

FIG. 3 (color online). (a) and (b): Weighted DCS for the charge exchange reaction $Na^+ + Rb(5p_{+1}) \rightarrow Na(4s) + Rb^+$ at $E = 1$ keV. The histograms are the measurements while the dashed (blue) and continuous (red) lines correspond to MOCC calculations including or omitting high-order multipole core-core interactions. (c): Corresponding left-right coherence parameter $A_\perp(\theta)$.

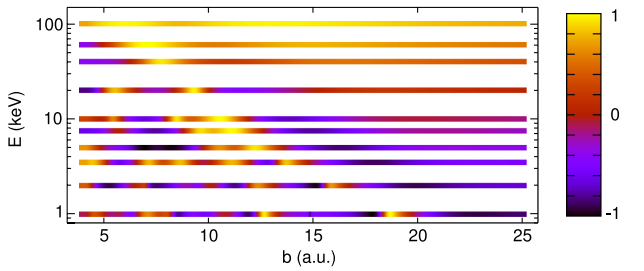

FIG. 4 (color online). $\mathcal{P}_{\pm1}(b)$ orientation parameter for the $5p_{+1} \rightarrow 3p$ right-hand capture process, as defined in Eq. (3), for selected impact energies E.

the ionic cores [28]. The improved calculations yield a maximum amplitude for the outer DCS peak at $\varphi = 0$, $\pi/2$, and $3\pi/2$ [Figs. 3(a) and 3(b)], in agreement with the measurements. In the case of capture into the $3p$ shell, which mostly occurs at large R ($R \gtrsim 15$ a.u.), changes with respect to the $1/R$ Coulombic interaction were found to be small because of the $1/R^4$ and $1/R^6$ behavior of the high-multipole interaction terms.

The asymmetry parameter associated with charge exchange into $4s$ directly measures the interference between radial $p_z \rightarrow s$ and rotational $p_x \rightarrow s$ pathways, since $A_\perp(\theta) = 2\,\mathrm{Im}(T_{p_z\rightarrow s}T^*_{p_x\rightarrow s})/[|T_{p_z\rightarrow s}|^2 + |T_{p_x\rightarrow s}|^2]$. The improved MOCC calculations enhance the agreement of the computed $A_\perp$ with experiment between $E\theta = 2$ and 3.5 eV · rad, which corresponds to the location of the outer DCS maximum. Beyond this range, the agreement deteriorates. In fact, the dipolar and quadrupolar core-core potentials introduced in the improved calculations induce strong oscillating phases in the expression for the scattering amplitudes T. These phases, which behave as $1/(vb^3)$ and $1/(vb^5)$, respectively, are essential to correctly reproduce the relative height of the DCS maxima, as previously observed, but diminish the outer part of the DCS upon integration over b. This results in a slight mismatch of the positions of the outer DCS maxima and leads to the deviation of $A_\perp$ with experiment at large θ. Improving further the theoretical calculations is beyond our present capabilities for such a complex system as $Na^+ + Rb$: ideally, *ab initio* calculations should be performed to explicitly represent the molecularization of the ionic cores at small R. This notwithstanding, the present improved MOCC calculations show overall a very satisfactory agreement with experiment.

We thus finally employ these MOCC calculations to gauge how well simple and intuitive pictures of orientation effects hold in the present low-energy charge exchange dynamics. A first picture is based on a velocity-matching model which predicts that capture preferentially occurs when the target's valence electron velocity coincides with the velocity direction of the passing ion [29,30]. Starting from $Rb(5p_{+1})$, this would mean that right-hand collisions should be favored and produce $Na(3p_{+1})$ within the $3p$ shell (Fig. 1). An alternative picture relies on the analysis of the phases entering the collisional amplitudes and prescribes that capture preferentially occurs if stationarity of the phases is possible over the effective interaction time. This gave rise to the so-called propensity rules [31,32] which would favor the $Rb(5p_{+1}) \rightarrow Na(3p_{-1})$ capture process for right-hand collisions. In order to discriminate between these (contradictory) predictions, we have computed the state-resolved orientation parameter

$$\mathcal{P}_{\pm1}(b) = \frac{P_{p_{+1}}(b,\pi) - P_{p_{-1}}(b,\pi)}{P_{p_{+1}}(b,\pi) + P_{p_{-1}}(b,\pi)}, \qquad (3)$$

where $P_{p_{\pm1}}(b,\varphi_b)$ are the anisotropic probabilities for the $Rb(5p_{+1}) \rightarrow Na(3p_{\pm1})$ reactions. $\mathcal{P}_{\pm1}(b)$ is represented in Fig. 4 for various impact energies ranging from 1 to 100 keV. For $E < 20$ keV, our results show that neither the velocity matching nor the propensity rules, which would lead to $\mathcal{P}_{\pm1} = +1$ and -1, respectively, apply. In this regime, the impact velocity is low enough to let the electron adapt almost adiabatically to the nuclear motion and the velocity matching criterion is not applicable. On the other hand, it is known that stationarity does not drastically determine the propensity in singly charged systems at low E [32]. However, as E increases, v approaches the target's electron velocity, and it is clearly seen in Fig. 4 that velocity matching prevails. This is quite satisfactory, as this model reflects well our intuitive understanding of charge exchange dynamics.

In conclusion, a MOTRIMS setup has been modified in order to explore low-energy atomic collisions with oriented targets. Consequently, asymmetry in the DCSs and related coherence properties have been observed with unprecedented resolution, not only for the main but also for secondary charge exchange channels. This has enabled not only the theoretical description to be improved but also marked out the limits of the single-active-electron and frozen-core approximations. Finally, we stress that the improved MOTRIMS protocol may similarly be employed to study other types of scattering dynamics at the coherence level with hitherto unsurpassed accuracy.

We thank Dr. Nigel Orr for his careful reading of our manuscript. We also acknowledge the computational facilities provided by the Mésocentre de Calcul Intensif Aquitain at University of Bordeaux [36].

[1] N. Andersen, J. W. Gallagher, and I. V. Hertel, Phys. Rep. **165**, 1 (1988).
[2] D. Dowek, J. Houver, J. Pommier, C. Richter, T. Royer, N. Andersen, and B. Palsdottir, Phys. Rev. Lett. **64**, 1713 (1990).
[3] Z. Roller-Lutz, Y. Wang, K. Finck, and H. O. Lutz, J. Phys. B **26**, 2697 (1993).
[4] J. W. Thomsen, I. Reiser, N. Andersen, J. C. Houver, J. Salgado, E. Sidky, A. Svensson, and D. Dowek, J. Phys. B **29**, 5459 (1996).
[5] S. Schippers, R. Hoekstra, R. Morgenstern, and R. E. Olson, J. Phys. B **29**, 2819 (1996).
[6] J. Salgado, J. W. Thomsen, N. Andersen, D. Dowek, A. Dubois, J. C. Houver, S. E. Nielsen, I. Reiser, and A. Svensson, J. Phys. B **30**, 3059 (1997).
[7] J. W. Thomsen, J. Salgado, N. Andersen, D. Dowek, A. Dubois, J. C. Houver, S. E. Nielsen, and A. Svensson, J. Phys. B **32**, 5189 (1999).
[8] Z. Roller-Lutz, Y. Wang, H. O. Lutz, S. E. Nielsen, and A. Dubois, Phys. Rev. A **61**, 022710 (2000).
[9] D. Dowek *et al.*, J. Phys. B **35**, 2051 (2002).
[10] A. G. Mikosza, J. F. Williams, and J. B. Wang, Phys. Rev. Lett. **79**, 3375 (1997).
[11] D. Cvejanovic, D. T. McLaughlin, and A. Crowe, J. Phys. B **33**, 3013 (2000).
[12] E. Goulielmakis *et al.*, Nature (London) **466**, 739 (2010).
[13] R. Dörner, V. Mergel, O. Jagutzki, L. Spielberger, J. Ullrich, R. Moshammer, and H. Schmidt-Böcking, Phys. Rep. **330**, 95 (2000).
[14] M. van der Poel, C. V. Nielsen, M. A. Gearba, and N. Andersen, Phys. Rev. Lett. **87**, 123201 (2001).
[15] J. Turkstra, R. Hoekstra, S. Knoop, D. Meyer, R. Morgenstern, and R. Olson, Phys. Rev. Lett. **87**, 123202 (2001).
[16] X. Fléchard, H. Nguyen, E. Wells, I. Ben-Itzhak, and B. D. DePaola, Phys. Rev. Lett. **87**, 123203 (2001).
[17] J. Blieck, X. Flechard, A. Cassimi, H. Gilles, S. Girard, and D. Hennecart, Rev. Sci. Instrum. **79**, 103102 (2008).
[18] A. Leredde, A. Cassimi, X. Fléchard, D. Hennecart, H. Jouin, and B. Pons, Phys. Rev. A **85**, 032710 (2012).
[19] I. Blank, S. Otranto, C. Meinema, R. E. Olson, and R. Hoekstra, Phys. Rev. A **85**, 022712 (2012); **87**, 032712 (2013).
[20] H. Nguyen, R. Brédy, X. Fléchard, and B. D. DePaola, J. Phys. B **46**, 115205 (2013).
[21] A. Dubois, S. E. Nielsen, and J. P. Hansen, J. Phys. B **26**, 705 (1993).
[22] M. Machholm, E. Lewartowski, and C. Courbin, J. Phys. B **27**, 4681 (1994); **27**, 4703 (1994).
[23] C. J. Lundy and R. E. Olson, J. Phys. B **29**, 1723 (1996).
[24] In practice, the left, up, right, and down contributions to the DCS are obtained by integrating $\sigma_{p_{+1}\to 3p}(\theta,\varphi)$ for fixed θ over the respective quadrants $\varphi = [-\pi/4, \pi/4]$ $[\pi/4, 3\pi/4]$, $[3\pi/4, 5\pi/4]$, and $[5\pi/4, 7\pi/4]$ (see Fig. 1). This considerably reduces the statistical noise in the measured profiles, but we have verified that the integrated contributions resemble those obtained for $\varphi = 0$, $\pi/2$, π, and $3\pi/2$, respectively.
[25] B. H. Bransden and M. H. C. McDowell, *Charge Exchange and the Theory of Ion-Atom Collisions* (Clarendon, Oxford, 1992).
[26] The polarizing setup induces a small shift of the target position, which slightly damages the MOTRIMS angular resolution. We could not systematically evaluate the resolution when the PLB is on, so we accordingly employed the optimal angular resolution (without PLB) for convolution purposes.
[27] At $E = 1$ keV, $A_\perp(\theta)$ could not be reliably derived from the measurements between $E\theta = 1.5$ and 2.5 eV $\cdot$ rad because of excessively noisy left and right signals.
[28] The values $\alpha_d^{\mathrm{Na}^+} = 0.9965$ a.u. and $\alpha_q^{\mathrm{Na}^+} = 0.376$ a.u. are taken from Ref. [33], while $\alpha_d^{\mathrm{Rb}^+} = 9.245$ a.u. and $\alpha_q^{\mathrm{Rb}^+} = 35.41$ a.u. are, respectively, issued from Refs. [34,35]. The ion-dipole and dipole-dipole interaction terms are naturally canceled at small R, where the total core-core interaction must be repulsive, since we introduce in our MOCC calculations a cutoff function which prevents the system from entering the R domain where the cores overlap [18].
[29] I. V. Hertel, H. Schmidt, A. Bahring, and E. Meyer, Rep. Prog. Phys. **48**, 375 (1985).
[30] E. E. B. Campbell, I. V. Hertel, and S. E. Nielsen, J. Phys. B **24**, 3825 (1991).
[31] S. E. Nielsen and N. Andersen, Z. Phys. D **5**, 321 (1987).
[32] J. P. Hansen, S. E. Nielsen, and A. Dubois, Phys. Rev. A **46**, R5331 (1992).
[33] J. C. Lombardi, Phys. Rev. A **32**, 2569 (1985).
[34] H. Coker, J. Phys. Chem. **80**, 2078 (1976).
[35] W. R. Johnson, D. Kolb, and K.-N. Huang, At. Data Nucl. Data Tables **28**, 333 (1983).
[36] http://www.mcia.univ-bordeaux.fr.